

UNCLASSIFIED

Defense Technical Information Center
Compilation Part Notice

ADP011770

TITLE: THz Imaging of Carrier Concentration and Mobility in Silicon

DISTRIBUTION: Approved for public release, distribution unlimited

This paper is part of the following report:

TITLE: International Conference on Terahertz Electronics [8th], Held in Darmstadt, Germany on 28-29 September 2000

To order the complete compilation report, use: ADA398789

The component part is provided here to allow users access to individually authored sections of proceedings, annals, symposia, etc. However, the component should be considered within the context of the overall compilation report and not as a stand-alone technical report.

The following component part numbers comprise the compilation report:

ADP011730 thru ADP011799

UNCLASSIFIED

THz Imaging of Carrier Concentration and Mobility in Silicon.

Michael Herrmann, Masahiko Tani, Kiyomi Sakai, Ryoichi Fukasawa

Abstract – Silicon samples have been imaged with THz radiation. The samples are n-type substrates, with half of one surface ion implanted with boron resulting in a $0.55 \mu\text{m}$ thin strongly p-doped layer. Silicon reflects and absorbs the THz beam due to a plasma resonance, subsequently the additional layer results in strong image contrast depending on the implantation dosage. Spectra of these samples have been fit using a refractive index and extinction coefficient calculated from the plasmon resonance: carrier concentration and relaxation time are used as adjustable parameters. By the fitting spectra at every image position, THz images of the carrier concentration and carrier mobility in silicon can be obtained.

I. INTRODUCTION

Silicon is one of the technologically most important materials today. It is also one of the most cleanly produced materials, and consequently the characterisation of silicon is an essential part of the silicon production process securing the quality of a delicate product. With the plasmon frequency of silicon in the THz regime, THz radiation should be suitable for optically determining the electrical properties of silicon. Some recent studies on silicon and other semiconductor spectra in the THz regime can be found in Refs. 1 - 5.

In 1995 it was demonstrated that THz frequency beams can be used in combination with a scanning technique providing local resolution of samples [6 - 8]. THz Imaging (also called "T-ray Imaging") may among other prospective applications serve as a convenient tool for the non-destructive, contactless and locally resolved characterisation of silicon and other semiconductors. The use of THz Imaging for semiconductor characterisation was first proposed by Mittleman *et al.* [8, 9] in 1996. They used a specialised THz Imaging setup with a magnetic field and a double detector system that makes use of the rotation of the polarisation of THz light due to the "terahertz Hall effect".

In this paper, we propose the characterisation of silicon with a standard THz Imaging setup. We investigate n- and p-type silicon, and a "thick" wafer as well as thin ion-implanted layers. The measurements are compared to analytic and computer-supported calculations.

M. Herrmann, M. Tani and K. Sakai are with the Communication Research Laboratory, Kansai Advanced Research Center, 588-2 Iwaoka, Nishi-ku, Kobe 651-2401, Japan

R. Fukasawa is with Tohigi Nikon Corp., 770 Midori, Ohtawara-shi, Tohigi 324-8625, Japan

II. EXPERIMENTAL

The optical setup used for the experiments is shown in Fig. 1. The output of a Ti:Sapphire laser is split into a pump and probe beam. The pump beam hits the THz emitter, a dipole antenna on LT-GaAs. The emitted THz radiation is focused with parabolic mirrors on the sample, which is scanned in two directions vertical to the beam. The transmitted radiation is focused on the THz receiver, another dipole antenna, which is gated by the probe beam. When a THz pulse and a probe pulse arrive at the receiver simultaneously, a signal is generated and recorded with a lock-in amplifier. The probe pulse can be delayed with a delay stage. In this way a time-domain waveform is recorded at every image position.

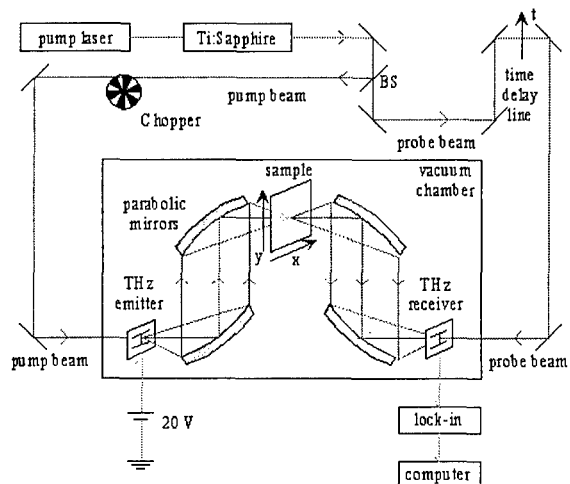


Fig. 1: Optical setup.

The samples are three specimen cut from a $380 \mu\text{m}$ thick, phosphorus-doped n-type Si wafer with $4.5 \Omega\text{cm}$ resistivity. Half of one surface of each sample has a $0.55 \mu\text{m}$ thin p⁺-type layer produced by ion-implanting boron at a dosage of $5 \times 10^{13} \text{ cm}^{-2}$, $5 \times 10^{14} \text{ cm}^{-2}$ or $5 \times 10^{15} \text{ cm}^{-2}$, respectively, and subsequent annealing.

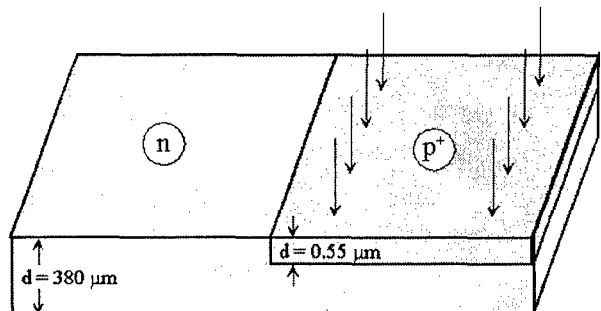


Fig. 2: Schematic of the sample. Half a surface has been ion-implanted with boron resulting in a p⁺-type layer.

III. INTENSITY-BASED IMAGES

In the intensity-based THz images, the non-implanted sides of the samples transmit between 40 to 50 % of the THz signal (i.e. electric field), and the implanted layers provide another drop in signal intensity that depends on the doping concentration. Fig. 3. shows a THz image of the $5 \times 10^{15} \text{ cm}^{-2}$ Si sample. On part of the image the THz beam was allowed to pass the sample. The corresponding (right-hand) part of the image is bright, representing maximum transmittance, or the reference level. The rest of the image shows two regions of different transmittance corresponding to the implanted (top) and the non-implanted (bottom) part of the sample. On all intensity-based images shown here, zero brightness (i.e. black) represents zero transmittance.

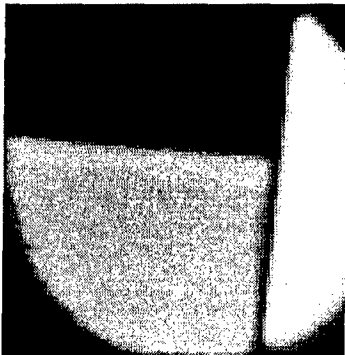


Fig. 3: THz image of the $5 \times 10^{15} \text{ cm}^{-2}$ Si sample. On the right-hand side the THz beam reaches the receiver directly, resulting in a strong signal. The sample (larger, left part of the image) reflects and absorbs the THz beam partly. The upper part of the sample is the implanted side. Image size is 20 mm \times 20 mm. The dark areas in the edges are shadows from the sample holder.

In Fig. 4 THz images of the three samples are compared. Their undoped sides look identical, but the doped sides differ according to doping concentration. The weakly implanted layer causes only a slight reduction in intensity, while the strongly doped layer reduces the THz signal by another factor 5. This is shown quantitatively in Fig. 5 which is based on vertical intersections through a set of images as those in Fig. 4.

IV. THEORY

The interaction between a semiconductor and electromagnetic radiation at THz frequencies is due to plasmon resonance and can be described by

$$\epsilon(\omega) = \epsilon_{\infty} - \frac{\epsilon_{\infty} \omega_p^2}{\omega^2 - i\omega\tau^{-1}} = \tilde{n}^2 = (n + ik)^2 \quad (1)$$

[10] where ω_p is the plasmon frequency with

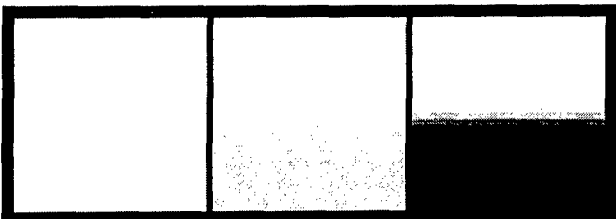


Fig. 4: Intensity-based THz images of three n-type Si samples the lower parts of which have been ion-implanted with boron, resulting in $0.55 \mu\text{m}$ thin p^+ -type layers. Implantation dosages (from left to right): $5 \times 10^{13} \text{ cm}^{-2}$, $5 \times 10^{14} \text{ cm}^{-2}$ and $5 \times 10^{15} \text{ cm}^{-2}$.

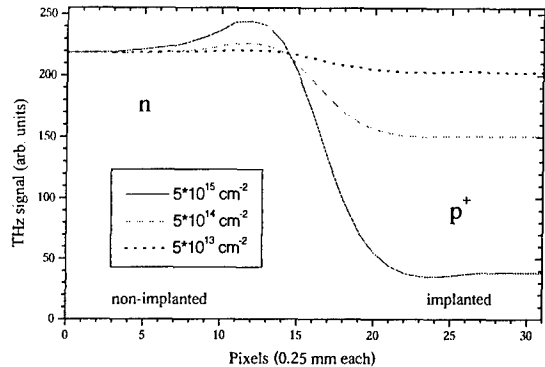


Fig. 5: Intersections through THz images of the three samples. While the 92 % of the THz electric field signal can transmit the weakly doped layer (dotted line), only 18 % pass through the strongly doped layer (solid line).

$$\omega_p^2 = \frac{Ne^2}{m^* \epsilon_0 \epsilon_{\infty}} \quad (2), \quad \tau = \frac{\mu m^*}{e} \quad (3) \text{ the relaxation or}$$

scattering time, ϵ (or ϵ_{∞}) the dielectric function (at infinite frequency, respectively), $\tilde{n} = n + ik$ the complex refractive index, and N , μ , m^* , e and ϵ_0 the carrier concentration, mobility, effective mass, electron charge and vacuum permittivity, respectively.

If the semiconductor properties are known, the complex refractive index can be calculated from Eq. 1, and transmittance through a single semiconductor layer can then be calculated using

$$t(\omega) = \frac{E_{\text{sample}}}{E_{\text{ref}}} = \frac{4\tilde{n}}{(\tilde{n}+1)^2} \times \frac{e^{i(\tilde{n}-1)\frac{\omega}{c}d}}{1 - \frac{(\tilde{n}-1)^2}{(\tilde{n}+1)^2} e^{2i\tilde{n}\frac{\omega}{c}d}} \quad (4)$$

[12] where the middle fraction describes reflection at the surfaces and in the right fraction the numerator represents bulk absorption and phase shift and the denominator takes account of multiple reflection.

For the implanted sides, a two-layer model has to be used as described by Eq. 5.

$$\frac{E_{\text{sample}}}{E_{\text{ref}}} = \frac{8\tilde{n}_1\tilde{n}_2}{(\tilde{n}_1+1)(\tilde{n}_1+\tilde{n}_2)(\tilde{n}_2+1)} \frac{e^{i(\tilde{n}_1-1)\frac{\omega}{c}d_1} e^{i(\tilde{n}_2-1)\frac{\omega}{c}d_2}}{1 + \alpha_1 + \alpha_2 + \alpha_3} \quad (5)$$

$$\text{with } \alpha_1 = \frac{(\tilde{n}_1-1)(\tilde{n}_2-\tilde{n}_1)}{(\tilde{n}_1+1)(\tilde{n}_2+\tilde{n}_1)} e^{2i\tilde{n}_1\frac{\omega}{c}d_1},$$

$$\alpha_2 = -\frac{(\tilde{n}_2-\tilde{n}_1)(1-\tilde{n}_2)}{(\tilde{n}_2+\tilde{n}_1)(1+\tilde{n}_2)} e^{2i\tilde{n}_2\frac{\omega}{c}d_2},$$

$$\alpha_3 = -\frac{(\tilde{n}_1-1)(1-\tilde{n}_2)}{(\tilde{n}_1+1)(1+\tilde{n}_2)} e^{2i\frac{\omega}{c}(\tilde{n}_1d_1+\tilde{n}_2d_2)}$$

[12]. However, much of what happens in the layer can also be understood from a thin-layer approximation of Eq. 4. For a given, constant implantation dosage N_{ar} , the carrier concentration $N = N_{ar}/d$ increases with decreasing thickness d , so that \tilde{n}^2 is proportional to $1/d$ in Eqs. 1 and 2. Using this and going towards zero thickness, Eq. 4 works out to

$$t_{thin}(\omega) = \frac{E_{sample}}{E_{ref}} = \frac{1}{1 + \frac{i}{2} \tilde{n}^2 \frac{\omega}{c} d} = \frac{1}{1 + \frac{N_{ar} e^2 \tau}{2cm^* \epsilon_0} (1 - i\omega\tau)} \quad (6)$$

In a strongly doped sample τ can drop to 10 fs and is then $\ll 1/\omega$ at THz frequencies, so that the imaginary part of Eq. 6 can be neglected in determining the absolute value of the transmittance. The phase shift can be calculated from Eq. 6 to be

$$\tan \varphi(\omega) = \frac{\text{Im}(t_{thin}(\omega))}{\text{Re}(t_{thin}(\omega))} = -\omega\tau, \quad (7)$$

in a further approximation valid for $N_{ar} \gg 10^{14} \text{ cm}^{-2}$ and thus at least for the strongly doped sample. Using these approximations the delay time in a thin layer equals minus the relaxation time, $\Delta t = \varphi(\omega)/\omega = -\tau$.

V. FITTING SPECTRA

Fig. 6 shows a three-parameter fit of THz transmittance for the non-implanted side using Eqs. 1 to 4. With $1960 \text{ cm}^2/\text{Vs}$ the resulting mobility is significantly higher than the literature value of $1450 \text{ cm}^2/\text{Vs}$ for intrinsic silicon. They are in fairly good agreement with those of van Exter *et al.* [1, 2] who also measure significantly increased values for μ . From the resulting values for N and μ , the resistivity is calculated to $\rho = 4.4 \text{ } \Omega\text{cm}$ which is in very good agreement with a value of $\rho = 4.5 \text{ } \Omega\text{cm}$ measured on this sample with spreading resistance technique.

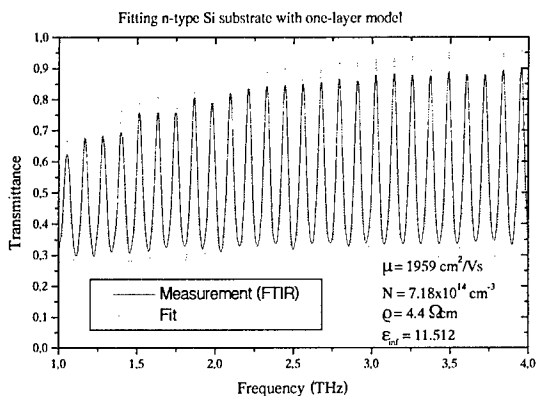


Fig. 6: A THz spectrum measured by Fourier Transform Infrared Spectrometry (FTIR) of the non-implanted side was fit using Eqs. 1 and 2.

In the thin layer approximation, the transmittance depends only on the product $N\mu$, not on N and μ separately (cf. Eqs. 3 and 6 with the imaginary part in Eq. 6 neglected). This is why only one of these two quantities can be fit from a transmittance spectrum. In order to fit the second quantity, phase information must be taken into account.

VI. TIME DELAY

Since the time delay is much smaller than the pulse duration, determining the time delay from specific features of the measured THz waveforms is questionable because even slight changes of pulse shape due to dispersion can change the result significantly. However, relatively good agreement is reached by Fourier

transforming the waveforms and calculating the time delay from the FFT phase shift at various frequencies. Fig. 7 shows a THz image based on time delay at 1.25 THz determined in this way. The delay of the implanted side relative to the non-implanted side amounts to -8.5 ± 2 fs. The calculated value is -6 fs. The calculation used Eq. 4 without the correction for multiple reflection for the non-implanted side and Eq. 5 for the implanted side. Multiple reflection in the substrate was excluded from the formulas, since the recorded time-domain waveforms were short and did not include pulses reflected through the substrate. Multiple reflection within the doped layer however was included.



Fig. 7: Time-delay THz image (17 mm \times 5 mm) of the strongly doped sample. The implanted region at the left appears dark representing earlier arrival time by 8.5 ± 2 fs. The dark vertical line in the middle is probably a diffraction effect.

VII. CONCLUSION

We have used a conventional THz Imaging system for investigating the local distribution of carrier concentration and mobility in silicon samples. n- and p-type silicon have been measured, and a "thick" wafer as well as thin ion-implanted layers. The measurements have been compared to analytic and computer-supported calculations. For a thick sample (i.e. $>$ several $10 \mu\text{m}$), both carrier concentration and mobility can be determined by fitting transmission spectra. Mobility data is significantly increased against the literature value, but we see excellent agreement with the nominal value of sample resistivity. For a thin layer, either concentration or mobility can be determined in this way, the other quantity being accessible via time-delay information. The time-delay of a $0.55 \mu\text{m}$ thin p⁺-type layer on n-type substrate has been determined to -8.5 ± 2 fs in fair agreement with calculations using a two-layer model. The method is non-destructive, does not need electric sample contacts and has a local lateral resolution of about 1 mm.

References

1. M. van Exter and D. Grischkowsky, "Carrier dynamics of electrons and holes in moderately doped silicon", *Phys. Rev. B* **41** (17), 12140 - 12142 (1989).
2. M. van Exter and D. Grischkowsky, "Optical and electronic properties of doped silicon from 0.1 to 2 THz", *Appl. Phys. Lett.* **56** (17), 1694 - 1696 (1990).
3. R. Fukasawa, K. Sakai and S. Perkowitz, "Far-Infrared Reflectance Study of Coupled Longitudinal-Optical Phonon-Hole Plasmon Modes and Transport Properties in Heavily Doped p-Type GaAs", *Jpn. J. Appl. Phys.* **36**, 5543 - 5548 (1997).
4. O. Morikawa, M. Tonouchi and M. Hangyo, "Sub-THz spectroscopic system using a multimode laser diode and photoconductive antenna", *Appl. Phys. Lett.* **75** (22), (1999).

5. O. Morikawa, M. Tonouchi and M. Hangyo, "A cross-correlation spectroscopy in sub-terahertz region using a incoherent light source", submitted to Appl. Phys. Lett. (2000).
6. B.B. Hu and M.C. Nuss, "Imaging with terahertz waves", Opt. Lett. **20**, 1716-1718 (1995).
7. Q. Wu, T.D. Hewitt and X.-C. Zhang, "Two-dimensional electro-optic imaging of THz beams", Appl. Phys. Lett. **69**, 1026-1028 (1996).
8. D.M. Mittleman, R.H. Jacobsen and M.C. Nuss, "T-ray Imaging", IEEE J. Quantum Electron. **2** (3), 679-692 (1996).
9. D.M. Mittleman, J. Cunningham, M.C. Nuss, "Noncontact semiconductor wafer characterisation with the terahertz Hall effect", Appl. Phys. Lett. **71** (1), 16-18 (1997).
10. Cf. textbooks that cover the interaction of light with matter, for instance Ref. 11.
11. D.F. Edwards, "Silicon (Si)", in E.D. Palik (ed.), "Handbook of Optical Constants of Solids", Academic Press, San Diego (1985, 1998).
12. Eqs. 4 and 5 can either be calculated from scratch using simple quantum mechanics for photons crossing a potential wall, or for instance using a formalism from M. Born and E. Wolf, "Principles of Optics", Cambridge University Press (1959, 1980).